Langmuir Article

pubs.acs.org/Langmuir

On-Chip Dielectrophoretic Coassembly of Live Cells and Particles into Responsive Biomaterials

Shalini Gupta,[†] Rossitza G. Alargova,[‡] Peter K. Kilpatrick,[§] and Orlin D. Velev*

Department of Chemical and Biomolecular Engineering, North Carolina State University, Raleigh, North Carolina 27695-7905. [†] Present address: Imperial College London, London, U.K. SW7 2AZ. [‡] Present address: Vertex Pharmaceuticals Inc., Cambridge, Massachusetts 02139-4242. [§] Present address: Department of Chemical and Biomolecular Engineering, University of Notre Dame, Notre Dame, Indiana 46556-5637.

Received August 11, 2009. Revised Manuscript Received October 10, 2009

We report how live cells and functionalized colloidal particles can be coassembled into a variety of freely suspended bioactive structures using dielectrophoresis on a chip. Alternating electric fields were applied to dilute suspensions of yeast (*S. cerevisiae*) and NIH/3T3 mouse fibroblast cells to yield 1D chains and 2D arrays. The effects of voltage, frequency, pH, electrolyte concentration, cell concentration, and particle size on the assembly process were investigated in detail. Numerical simulations of the field intensity and energy allow the capture of the dynamics of cell−cell and cell−particle assembly. The simulation results illustrate that the electric field draws the functionalized synthetic particles between the cells and enables the formation of permanent chains and monolayer membranes composed of alternating cells and particles. The cell structures were bound into permanent structures by different types of functionalized synthetic particles and ligands that attached to the cells through biospecific or electrostatic interactions. The technique allowed the fabrication of magnetically responsive biomaterials that could be manipulated and transported into and out of the microchambers where they were formed.

1. Introduction

Biomaterials incorporating live cells offer unique advantages for comprehensive biosensing in comparison to the traditional detection strategies using the recognition of a single type of biomolecule (such as proteins, DNA, phospholipids, etc.).[1−4] A large number of previous studies report that live cellular arrays can be assembled on 2D substrates that have been templated using photolithographic microfabrication techniques or by microcontact printing of oligopeptides.[5−9] Cells from one or more different populations can also be patterned in stripes using laminar flow patterning in microfluidic devices.[6,10] Other methods for the fabrication of cell-based biomaterials make use of dip-pen nanolithography,[11,12] convective assembly,[13,14] cell adhesion and infusion to porous polymeric scaffolds and polyelectrolyte multilayers,[15−18] and the encapsulation of cells in poly(ethylene glycol) (PEG)-based hydrogels.[19,20] These techniques, however, typically lack the flexibility of preparing freely suspended structures from cells, such as chains or membranes. A few studies describe the formation of free-floating assemblies composed of synthetic particles functionalized by biomolecules.[21−27] These methods may not be easily applied to making structures from live cells, which are large, sediment rapidly, and are more difficult to manipulate and guide toward assembly.

Electric fields allow rapid on-chip manipulation of cells in suspensions using dielectrophoresis (DEP).[28−34] DEP is defined

*Corresponding author. E-mail: odvelev@unity.ncsu.edu. Phone: 919-513-4318.

(1) Anderson, D. G.; Levenberg, S.; Langer, R. *Nat. Biotechnol.* **2004**, *22*, 863–866.
(2) Langer, R.; Tirrell, D. A. *Nature* **2004**, *428*, 487–492.
(3) Willner, I. *Science* **2002**, *298*, 2407–2408.
(4) Katz, E.; Willner, I. *Angew. Chem., Int. Ed.* **2004**, *43*, 6042–6108.
(5) Bhatia, S. K.; Hickman, J. J.; Ligler, F. S. *J. Am. Chem. Soc.* **1992**, *114*, 4432–4433.
(6) Kane, R. S.; Takayama, S.; Ostuni, E.; Ingber, D. E.; Whitesides, G. M. *Biomaterials* **1999**, *20*, 2363–2376.
(7) Quist, A. P.; Pavlovic, E.; Oscarsson, S. *Anal. Bioanal. Chem.* **2005**, *381*, 591–600.
(8) Park, A.; Wu, B.; Griffith, L. G. *J. Biomater. Sci., Polym. Ed.* **1998**, *9*, 89–110.
(9) Ghosh, P.; Amirpour, M. L.; Lackowski, W. M.; Pishko, M. V.; Crooks, R. M. *Angew. Chem., Int. Ed.* **1999**, *38*, 1592–1595.
(10) Takayama, S.; McDonal, J. C.; Ostuni, E.; Liang, M. N.; Kenis, P. J. A.; Ismagilov, R. F.; Whitesides, G. M. *Proc. Natl. Acad. Sci. U.S.A.* **1999**, *96*, 5545–5548.
(11) Lee, K.-B.; Park, S.-J.; Mirkin, C. A.; Smith, J. C.; Mrksich, M. *Science* **2002**, *295*, 1702–1705.
(12) Demers, L. M.; Ginger, D. S.; Park, S.-J.; Li, Z.; Chung, S.-W.; Mirkin, C. A. *Science* **2002**, *296*, 1836–1838.
(13) Kahraman, M.; Yazici, M. M.; Sahin, F.; Culha, M. *Langmuir* **2008**, *24*, 894–901.
(14) Jerrim, L. B.; Velev, O. D. *Langmuir* **2009**, *25*, 5692–5702.
(15) Stevens, M. M.; Mayer, M.; Anderson, D. G.; Weibel, D. B.; Whitesides, G. M.; Langer, R. *Biomaterials* **2005**, *26*, 7636–7641.
(16) Khademhosseini, A.; Langer, R.; Borenstein, J.; Vacanti, J. P. *Proc. Natl. Acad. Sci. U.S.A.* **2006**, *103*, 2480–2487.
(17) Jaber, J. A.; Schlenoff, J. B. *Curr. Opin. Colloid Interface Sci.* **2006**, *11*, 324–329.
(18) Griffith, L. G.; Naughton, G. *Science* **2002**, *295*, 1009–1014.
(19) Albrecht, D. R.; Tsang, V. L.; Saha, R. L.; Bhatia, S. N. *Lab Chip* **2005**, *5*, 111–118.
(20) Mahoney, M. J.; Anseth, K. S. *Biomaterials* **2006**, *27*, 2265–2274.
(21) Tirrell, M.; Kokkoli, E.; Biesalski, M. *Surf. Sci.* **2002**, *500*, 61–83.
(22) Hiddessen, A. L.; Rodgers, S. D.; Weitz, D. A.; Hammer, D. A. *Langmuir* **2000**, *16*, 9744–9753.
(23) Singh, H.; Laibinis, P. E.; Hatton, T. A. *Langmuir* **2005**, *21*, 11500–11509.
(24) Dreyfus, R.; Baudry, J.; Roper, M. L.; Fermigier, M.; Stone, H. A.; Bibette, J. *Nature* **2005**, *437*, 862–865.
(25) Snoswell, D. R. E.; Brill, R. K.; Vincent, B. *Adv. Mater.* **2007**, *19*, 1523−1527.
(26) Lin, Y.; Skaff, H.; Böker, A. B.; Dinsmore, A. D.; Emrick, T.; Russell, T. P. *J. Am. Chem. Soc.* **2003**, *125*, 12690–12691.
(27) Tang, Z.; Zhang, Z.; Wang, Y.; Glotzer, S. C.; Kotov, N. A. *Science* **2006**, *314*, 274–278.
(28) Velev, O. D.; Bhatt, K. H. *Soft Matter* **2006**, *2*, 738–750.
(29) Alp, B.; Stephens, G. M.; Markx, G. H. *Enzyme Microbiol. Technol.* **2002**, *31*, 35–43.
(30) Chiou, P. Y.; Ohta, A. T.; Wu, M. C. *Nature* **2005**, *436*, 370–372.
(31) Pethig, R.; Markx, G. H. *Trends Biotechnol.* **1997**, *15*, 426–432.
(32) Pethig, R.; Huang, Y.; Wang, X.-B.; Burt, J. P. H. *J. Phys. D: Appl. Phys.* **1992**, *24*, 881–888.
(33) Gong, T.; Wu, D. T.; Marr, D. W. M. *Langmuir* **2003**, *19*, 5967–5970.
(34) Gong, T.; Marr, D. W. M. *Langmuir* **2001**, *17*, 2301–2304.

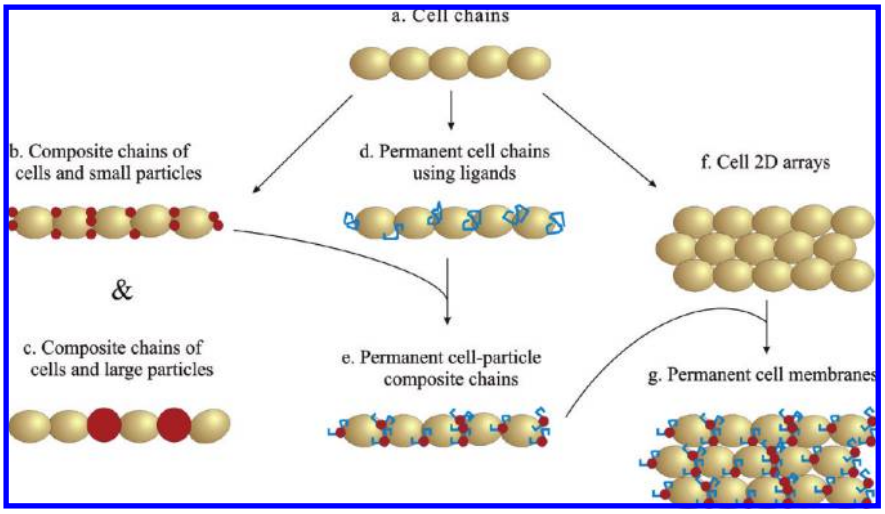

Figure 1. Schematic of the various classes of cell−cell and cell−particle assemblies formed using dielectrophoresis in ac electric fields.

as the mobility of dielectric particles in a medium imparted by spatially nonuniform electric fields.[35,36] The use of alternating current (ac) electric fields in DEP, in particular, allows the precise, controlled organization of particles without causing water electrolysis and electroosmotic effects. When an ac field with frequency of ω is applied across a colloidal suspension, it leads to the polarization of particles. The dipoles induced in the particles interact with the applied electric field, giving rise to DEP. The magnitude of the dielectrophoretic force is proportional to the gradient of the electric field intensity squared.

$$F_{\mathrm{DEP}} = 2\pi\varepsilon_{\mathrm{m}}R^3 Re|K(\omega)|\nabla {E_{\mathrm{rms}}}^2 \quad (1)$$

Here, ε_{m} is the dielectric permittivity of the medium, R is the particle radius, E is the electric field intensity, and K is the Clausius−Mossotti function—the effective polarizability of the particle in the medium. The real part of K is given by

$$Re|K(\omega)| = \frac{\varepsilon_{\mathrm{m}} - \varepsilon_{\mathrm{p}}}{\varepsilon_{\mathrm{m}} + 2\varepsilon_{\mathrm{p}}} + \frac{3(\varepsilon_{\mathrm{p}}\sigma_{\mathrm{m}} - \varepsilon_{\mathrm{m}}\sigma_{\mathrm{p}})}{\tau_{\mathrm{MW}}(\sigma_{\mathrm{m}} + 2\sigma_{\mathrm{p}})^2(1 + \omega^2{\tau_{\mathrm{MW}}}^2)} \quad (2)$$

where ε_{p} is the dielectric permittivity of the particle and $\sigma_{\mathrm{m,p}}$ represents the conductivities of the medium and particles, respectively. The $Re|K(\omega)|$ function changes sign at a crossover frequency of $\omega_{\mathrm{c}} = {\tau_{\mathrm{MW}}}^{-1}$, where $\tau_{\mathrm{MW}} = (\varepsilon_{\mathrm{m}} + \varepsilon_{\mathrm{p}})/(\sigma_{\mathrm{m}} + 2\sigma_{\mathrm{p}})$ is the Maxwell−Wagner charge-relaxation time. When $Re|K(\omega)| > 1$, the particles are attracted to the region of maximum field intensity and the phenomenon is known as positive DEP. Particles with lower polarizability than the medium are repelled from the high-field-intensity areas by negative DEP.

The dipoles induced in the particles by the ac field also exert attractive forces between particles and cause them to align into chains. The magnitude of this particle-chaining force is proportional to the square of the field intensity and is given by

$$F_{\mathrm{chain}} = -C\pi\varepsilon_{\mathrm{m}}R^2 Re|K(\omega)|^2E^2, \quad 3 < C < 10^3 \quad (3)$$

where the coefficient C depends on the distance between the particles and the length of the particle chain. The combination of DEP and particle chaining can be used as a facile tool for the directed colloidal assembly of microscopic functional structures.[37] A few examples of functional particle structures assembled by dielectrophoresis include miniaturized biosensors,[38,39] electrically conductive microwires from gold nanoparticles,[40−42] and switchable particle crystals for photonic applications.[43−45]

We describe here in depth a method in which the principles of directed on-chip colloidal assembly are transcribed into the biological domain by effectively treating the live cells as "smart" or functional particles.[46] Dilute suspensions of eukaryotic yeast and fibroblast cells are subjected to nonuniform ac electric fields on a chip and are assembled into chains or 2D membranes using DEP. The mere assembly of cells between the electrodes is, however, not enough to form a functional material or device component because the cells are electrostatically charged and the inherent cell−cell interactions are weak so the structures disassemble when the electric field is switched off. We demonstrate both experimentally and by simulations that the permanent binding of freely suspended cell structures can be accomplished by using surface-functionalized microparticles that are drawn between the cells by electric fields and attach to the cell surfaces via electrostatic and/or biospecific interactions. The wide range of cell structures that we assemble is schematically outlined in Figure 1 in increasing order of complexity. By using lectin-functionalized paramagnetic microparticles, we also illustrate how the biological functionality of the cell assemblies can be augmented by the physical functionality of the binder particles to make novel and responsive biomaterials. The effects of various operating parameters on the cell-assembly process are evaluated in detail and discussed.

2. Experimental Section

Materials and Sample Preparation. Dried, active brewer's yeast (*Saccharomyces cerevisiae*) was purchased from MP

(35) Jones, T. B. *Electromechanics of Particles*; Cambridge University Press: Cambridge, U.K., 1995.
(36) Pohl, H. A. *Dielectrophoresis*; Cambridge University Press: Cambridge, U.K., 1978.

(37) Velev, O. D.; Gupta, S. *Adv. Mater.* **2009**, *21*, 1897–1905.
(38) Velev, O. D.; Kaler, E. W. *Langmuir* **1999**, *15*, 3693–3698.
(39) Park, S.-J.; Taton, T. A.; Mirkin, C. A. *Science* **2002**, *295*, 1503–1506.
(40) Hermanson, K. D.; Lumsdon, S. O.; Williams, J. P.; Kaler, E. W.; Velev, O. D. *Science* **2001**, *294*, 1082–1086.
(41) Bhatt, K. H.; Velev, O. D. *Langmuir* **2004**, *20*, 467–476.
(42) Lumsdon, S. O.; Scott, D. M. *Langmuir* **2005**, *21*, 4874–4880.
(43) Lumsdon, S. O.; Kaler, E. W.; Williams, J. P.; Velev, O. D. *Appl. Phys. Lett.* **2003**, *82*, 949–951.
(44) Lumsdon, S. O.; Kaler, E. W.; Velev, O. D. *Langmuir* **2004**, *20*, 2108–2116.
(45) Gangwal, S.; Cayre, O. J.; Velev, O. D. *Langmuir* **2008**, *24*, 13312–13320.
(46) Gupta, S.; Alargova, R. A.; Kilpatrick, P. K.; Velev, O. D. *Soft Matter* **2008**, *4*, 726–730.

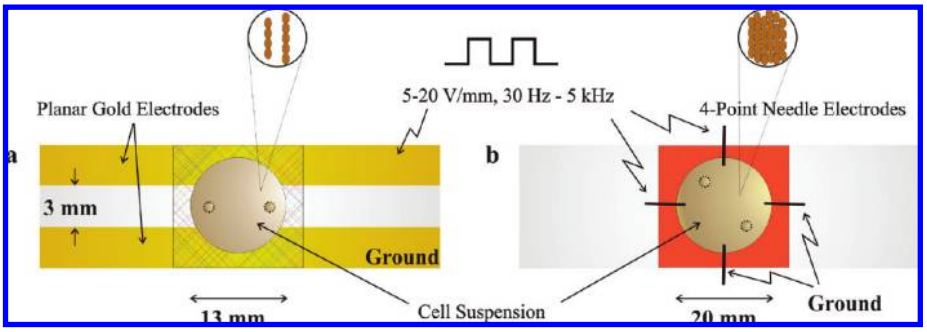

Figure 2. Schematics of the chips used for the dielectrophoretic assembly of live cells: (a) Parallel coplanar gold electrodes for making 1D chains and (b) chamber with orthogonally arranged four-point brass electrodes used to fabricate uniform 2D arrays.

Biomedicals, Inc. (OH). Phosphate-buffered saline (PBS) tablets were purchased from Sigma-Aldrich (MO). A PBS solution containing 0.1 mM phosphate buffer, 1.37 mM NaCl, and 0.027 mM KCl was prepared by dissolving 1 PBS tablet in 20 L of deionized (DI) water with a resistivity of ~18.2 MΩ cm (Millipore RiOs purification system, MA). The yeast cells were suspended in PBS to obtain final concentrations between 0.05 and 0.2% w/v at pH 6.3. NIH/3T3 mouse fibroblast cells were cultured in standard Dulbecco's Modified Eagle's Medium (Gibco/Invitrogen, CA) for 2 days. The cells were trypsinized and resuspended in an isotonic solution of 0.45 M dextrose (anhydrous, ACS certified; Fisher Scientific, PA) in DI water containing 1% v/v calf serum (Gibco/Invitrogen, CA) at pH 7.2.

The following types of monodisperse colloidal particles were used in the experiments: white sulfate-stabilized polystyrene latex spheres of 1.0 and 5.0 μm diameters (Interfacial Dynamics Corp., OR), fluorescent aldehyde/sulfate latex beads of 1.0 μm diameter (Molecular Probes, OR), amine-terminated magnetic iron oxide particles of 1.8 μm diameter (Bangs Laboratory, IN), and concanavalin A lectin-coated paramagnetic particles of 0.95 μm diameter (Spherotech, Inc., IL). The particles were centrifuged and washed twice with PBS using a Marathon micro-A centrifuge (Fisher Scientific) to remove any surfactants, electrolytes, or preservatives from the medium. For some experiments, the microparticles were further conjugated with proteins: (a) 1.0 μm aldehyde/sulfate latex beads and 1.8 μm amine-terminated magnetic particles were functionalized with fluorescein isothiocyanate (FITC)-labeled concanavalin A lectin (Sigma-Aldrich) and (b) 1.0 μm sulfate-stabilized latex spheres were modified with fibronectin (BD Biosciences, NJ). (See Supporting Information for coupling protocols.)

The microspheres were added to the cell suspensions to obtain samples with final particle concentrations between 0.01 and 0.1% w/v. Extrapure 96% $CaCl_2$ (Acros Organics, NJ) was added to the cell−particle mixtures to a concentration of 0.15 mM to facilitate the binding of the lectins to polysaccharides.[47] Bovine serum albumin (Sigma-Aldrich) and nonionic surfactant Tween 20 (Ted Pella, Inc., CA) were each included in approximate quantities of 0.1% w/v to prevent the nonspecific aggregation or adhesion of cells or particles. Other reagents used include protein-sequencing-grade 20.2% hydrochloric acid and cell-culture-tested 1.0 N sodium hydroxide (Sigma-Aldrich), D-mannose (Alfa Aesar, MA), and low-molecular-weight poly(dimethyl aminoethyl methacrylate) (synthesized in the laboratory).

Experimental Setup. The chaining experiments were performed between two coplanar gold electrodes with a ~3 mm gap (Figure 2a) that were vapor deposited onto 25 × 75 mm^2 plain microscope glass slides (Fisher Scientific) as described elsewhere.[41,46] The gold-coated slides were cleaned by immersing in NoChromix (Godax Laboratories, MD) overnight and then by washing with DI water, followed by air drying. The electrodes were encapsulated in a 0.15 mm thin, transparent flow chamber (HBW13, Grace Bio-Labs, OR). The setup for assembling 2D arrays consisted of four brass needle electrodes orthogonally arranged around the sides of a 2-mm-thick transparent flow chamber (PC1R-2.0, Grace Bio Laboratories) that was sealed on a glass slide as shown in Figure 2b.

The inner surfaces of the chips and microfluidic chambers were treated with 0.5% F-127 Pluronic surfactant (Molecular Probes) for 45 min prior to performing the experiments. This treatment was necessary to hydrophilize the surface and minimize the nonspecific interactions of the cells and particles with the substrate. Cell−particle suspensions were injected into the microfluidic flow chambers, and the electrodes were connected to a 33120A 15-MHz square-wave field function generator (Agilent Technologies, CO) providing an ac signal of 2−10 V peak to peak. The generated signal was amplified to a working voltage range of 15−200 V using an RG-91 voltage amplifier (Burleigh Instruments, NY). A 1 μF capacitor was connected in series to filter out any direct current (dc) component of the signal. The strength of the applied field was measured using a multimeter (Instek, CA) included in the circuit. Electric fields with intensities between 5 and 20 V mm^{-1} and frequencies between 30 Hz and 5 kHz were applied to the samples at room temperature.

Microscopy and Image Analysis. The assembly process was continuously monitored (top down) using an Olympus BX-61 optical microscope equipped with a transmitted- and fluorescence-mode microscope. The images were recorded using an Olympus DP-70 digital CCD camera. To characterize and compare the effects of the operating parameters, an electric field was applied for 2 min under each experimental condition and at least five representative high-magnification optical microscopy images (typically with a 50× objective) were collected from near the middle areas of the chamber away from the electrodes. Each point reported is an average of the data from these images.

The electron microscopy samples of the permanent membrane comprising yeast cells and lectin-functionalized paramagnetic particles were prepared after transfer onto a Nochromix-cleaned glass coverslip. The membrane was washed twice using DI water in order to remove any excess BSA, surfactant, unbound cells, and unbound lectin-functionalized particles from the media. The cells were fixed in 2% w/v glutaraldehyde for 2 to 3 h and then dehydrated by washing with a series of progressively concentrated ethanol solutions (20, 40, 60, 70% v/v) for 10 min each. They were finally left inside the 95% ethanol solution for ~1 h. The cells were dried using a carbon dioxide critical-point dryer. The dried samples were immediately mounted on top of a SEM stub and stored in a desiccator overnight. The samples were sputtered with a thin layer of gold (~10 Å) and then viewed with an FESEM (JEOL 6400F) using a 5 kV accelerating voltage.

Cell Viability Tests. The fluorescence tests for yeast cell viability were performed using FUN-1 cell stain (Molecular Probes). The dye stored at −20 °C was brought to room temperature and centrifuged at 975*g* for 5 min. Approximately 0.2 μL of the dye was mixed homogeneously with 200 μL of the 0.1% w/v yeast cells in PBS. The mixture was kept in the dark for 30 min,

(47) Stratford, M. *Yeast* **1989**, *5*, 487–496.

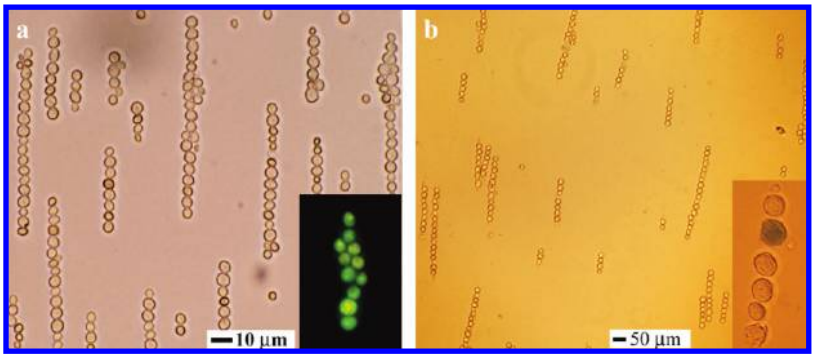

Figure 3. Optical micrographs of chains assembled from live cells using ac electric fields. (a) Yeast (*S. cerevisiae*) cell chains under 15 V mm^{-1} and a 50 Hz electric field. (Inset) The viability of the cells is preserved in the electric field after 2 h as indicated by the compartmentalized appearance of the cell interior. (b) NIH/3T3 mouse fibroblast cells under 10 V mm^{-1} and a 10 kHz electric field. (Inset) The blue color indicates a dead cell. Most cells remain viable during the assembly process for up to 1 h.

and the cells were then observed using fluorescence microscopy with the FITC filter set. The viability experiments for NIH/3T3 mouse fibroblast cells were performed using Trypan blue cell stain (Sigma). Trypan blue was dissolved in PBS at ~0.4% w/v concentration and was slowly added to the fibroblast cell suspension until a clear, light-blue suspension was obtained. The cells were viewed with transmitted-mode optical microscopy after 5 min.

3. Results and Discussion

The freely suspended cells in the buffer began aligning and assembling within 30 s of applying the ac electric field to the coplanar electrodes (Figure 3). The field in most of the volume between the electrodes is homogeneous and does not lead to cell motion because of macroscale gradient effects such as long-range DEP or related ac electrokinetic fluid motion. Only a minor fraction of the cells in the vicinity (tens of micrometers) of the electrodes were pulled into the region of maximum field intensity at the electrode edges by positive DEP[35] and ac electrohydrodynamics.[48] The major fraction of the yeast cells in the bulk of the experimental chamber assembled in chains in the direction of the applied electric field due to the attractive axial dipolar interactions and most cells were captured into chains in 10−15 min. This pattern of chain formation in electric fields is typical of colloidal suspensions in many different systems.[46,48−52] The process of cell chaining was accompanied by the slow sedimentation of the cells toward the bottom of the chip. The assembly process was reversible, and the cell chains came apart when the field was turned off. The cells then slowly redistributed because of Brownian motion but remained on the bottom surface of the chip because of gravity (Peclet number for yeast cells, $Pe \approx 40$).[53]

Cell Viability under Electric Fields. Our first goal at this stage was to check whether the viability of cells is preserved when the electric field is applied. We used FUN-1 cell stain to distinguish live yeast cells from dead ones; the display of orange-red fluorescent intravacuolar structures in a dull-green cytoplasm indicates metabolically active cells whereas the dead cells are bright fluorescent green-yellow. The proportion of metabolically active cells (~90%) remained approximately constant before and after applying the ac field for approximately 2 h, confirming that the electric field does not affect the viability of yeast cells under our experimental conditions (Figure 3a, inset).

The viability experiments for mouse fibroblast cells were performed using Trypan blue dye that penetrates only the cytoplasm of cells whose membranes are damaged. The cells that absorb the dye turn different shades of blue, and this allows us to monitor the health of the cells in real time. These observations were made from the time the cells were trypsinized and resuspended in the new buffer media. In the absence of an electric field, approximately 90% of the fibroblast cells stayed alive for up to 1−1.5 h at room temperature. No detectable change in the viability of fibroblasts was noted when an external electric field of up to 15 V mm^{-1} was applied (Figure 3b, inset). In general, fibroblast cells are more susceptible to small changes in their environment (such as temperature, pH, CO_2 content, electrolyte concentration, and others) than to the applied electric field. To prolong the viability of fibroblast cells, in the future these experiments may be performed inside a closed plastic chamber maintained at 37 °C and under a constant supply of 5% CO_2. Overall, the experiments prove that both yeast and fibroblast cells retain their metabolic activity after treatment on the DEP chips, at least for the time periods studied here.

Effect of Operating Parameters on the Assembly of Cell Chains. After proving that cells preserve their viability during DEP treatment, we identified and characterized the experimental parameters that affect the mechanism and the rate of cell chaining, including voltage and frequency of the electric field, pH of the suspension, electrolyte concentration in the buffer media, and concentration of cells in the suspension. The experimental results and the conclusions drawn are given below.

Effect of Field Strength and Frequency. The dielectrophoretic response of yeast cells was explored as a function of both field strength and frequency (Figure 4). First, an ac field of 20 V was applied to a 0.1% w/v yeast cell suspension, and the frequency was varied systematically from 10 Hz to 5 kHz in increments of 200 Hz or more. All other parameters were held constant. The cells that were captured in chains of varying lengths were counted using Image-Pro Plus analyzing software (Media Cybernetics, MD) and the average chain length was determined at each frequency. The procedure was repeated at 30, 40, 50, and 55 V.

The effect of voltage on cell assembly was straightforward. When the voltage was increased, the average cell chain length

(48) Green, N. G.; Morgan, H. *AC Electrokinetics: Colloids and Nanoparticles*; Research Studies Press: Hertfordshire, U.K., 2003.
(49) Llamas, M.; Giner, V.; Sancho, M. *J. Phys. D: Appl. Phys.* **1998**, *31*, 3160–3167.
(50) Ross, R. S.; Pincus, P.; Wudl, F. *J. Phys. Chem.* **1992**, *96*, 6169–6172.
(51) Butter, K.; Bomans, P. H. H.; Frederik, P. M.; Vroege, G. J.; Philipse, A. P. *Nature* **2003**, *2*, 88–91.
(52) Gast, A. P.; Zukoski, C. F. *Adv. Colloid Interface Sci.* **1989**, *30*, 153–202.
(53) The random displacement of the yeast cells due to Brownian motion was compared to their sedimentation due to gravity by calculating the Peclet number, which is given by $Pe=hU/D=(2\Delta\rho g h r^2/9\mu)/(k_B T/6\pi\mu r)$. Here, h is the characteristic displacement (assumed to be on the order of the cell diameter), U is the sedimentation velocity, D is the cell diffusion coefficient, $\Delta\rho$ is the difference in the densities, g is the acceleration due to gravity, r is the cell radius, μ is the medium viscosity, k_B is the Boltzmann constant, and T is the temperature.

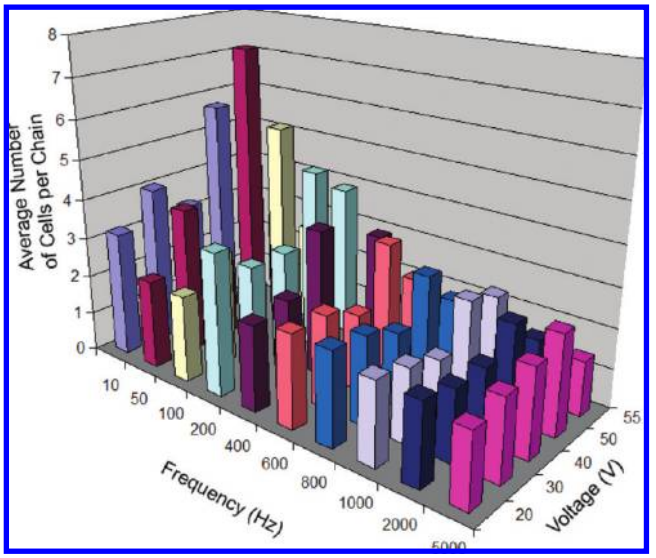

Figure 4. Effect of the ac electric field frequency and voltage on the length of the assembled yeast cell chains. Longer chains are formed at higher voltages and lower frequencies. Each data point is an average of data from 10 different images.

increased at all frequencies because the strength of the electric field is the main driving force for dielectrophoretic assembly. In principle, longer chains can be formed at even higher voltages, but this was not practical because increasing the voltage above 55 V resulted in water electrolysis and ac electro-osmotic flows.

Frequency had the opposite effect on cell assembly such that the chain lengths increased as the frequency decreased. No readings could be taken below 10 Hz because the cells vibrated as a result of electrophoretic mobility. The electrohydrodynamic flows of the bulk fluid also became significant at such low frequencies. These data correspond well to the concept that cells (and colloidal particles) show a large dispersion in the low-frequency range referred to as α dispersion in biophysics or low-frequency dielectric dispersion (LFDD) in colloidal chemistry.[47] This dispersion is related to the macroscopic polarization of the induced double layer around the cells and has a characteristic relaxation frequency of

$$\omega_{\text{char}} = \frac{2DM}{R^2} \tag{4}$$

where D is the diffusion coefficient of the ions in the double layer and M is a dimensionless factor that accounts for the electro-osmotic contribution of the ion flux of the double layer.

At pH 6.3, the yeast cells are negatively charged (the isoelectric point of yeast cells is pH 4)[54,55] and are surrounded by positive counterions, mostly Na^+ in our medium. When an external field is applied, the counterions outside and the ions inside the cell polarize in a frequency-dependent manner. The dipole magnitude decreases as the frequency increases above the characteristic relaxation frequency. Using eq 4 and the physical parameters reported in Table 1, the characteristic relaxation frequency for the yeast cells in our medium was calculated to be $\omega_{\text{char}} \cong 800$ Hz, which is consistent with the decreased cell chain length observed at higher frequencies (Figure 4). The zeta potential of the cells was estimated from the electrophoretic mobility data reported in the literature.[54,56] This value of the zeta potential was then used to calculate the cell's surface charge density using the simplified Grahame equation.[47] The values of all other parameters were either calculated under the given experimental conditions or based on values listed in the literature.[47]

Table 1. List of Physical Parameters Used for the Calculation of the Characteristic Relaxation Frequency of Yeast Cells

	physical parameters	values	units
R	cell radius	2.5×10^{-6}	m
D	diffusion coefficient of Na^+	1.33×10^{-9}	$m^2\ s^{-1}$
q	elementary electron charge	1.6×10^{-19}	C
σ_q	surface charge density	1.77×10^{-3}	$C\ m^{-2}$
k_B	boltzmann constant	1.38×10^{-23}	$J\ K^{-1}$
T	temperature	298	K
ε_0	permittivity of free space	8.85×10^{-12}	$C^2\ J^{-1}\ m^{-1}$
ε_m	permittivity of the medium	7.08×10^{-10}	$F\ m^{-1}$
κ	1 Debye length	1.04×10^{8}	m^{-1}
ζ	zeta potential	−0.017	V
$C'_d = \varepsilon_m\kappa \cos(q\zeta/2k_BT)$	effective capacitance of the bound layer	7.78×10^{-2}	$F\ m^{-2}$
$M = 1 + (q\sigma_q/k_BTC'_d)$	dimensionless factor	1.89	

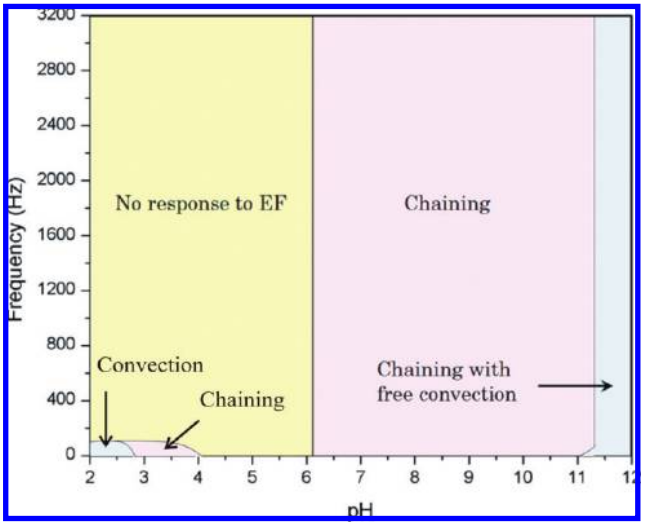

Figure 5. Effect of pH and frequency on the types of structures formed by the dielectrophoretic assembly of yeast cells. The electric field intensity was 10 V mm^{-1}.

Effect of pH on the Chaining Efficiency. The effect of frequency on the rate of cell chaining highlighted the importance of the counterionic layer around the cells yielding the induced dipole polarization. The counterionic charge and resulting polarization can be changed by the pH of the cell suspension; therefore, the pH is expected to be another key parameter controlling the DEP assembly process. We characterized the effect of pH on cell chaining at different frequencies by varying the pH of a 0.1% w/v yeast cell suspension from pH 2.8 to 11.5 in increments of approximately 0.7 unit using 1 N HCl or 1 N NaOH (Figure 5). The applied electric field strength was 10 V mm^{-1}. No dielectrophoretic movement of the cells was observed below pH ~6; however, electrohydrodynamic flows caused some cells to align near the electrodes at low frequencies between pH 3 and 4. The cells readily organized into chains above pH 6.2, but the rate of cell assembly decreased as the frequency was increased, which is

(54) Ahimou, F.; Denis, F. A.; Touhami, A.; Dufrene, Y. F. *Langmuir* **2002**, *18*, 9937–9941.
(55) Narong, P.; James, A. E. *Colloids Surf., A* **2006**, *274*, 130–137.
(56) Baran, A. A. *Adv. Colloid Interface Sci.* **1998**, *75*, 45–78.

 DOI: 10.1021/la902989r E

consistent with our previous frequency results. Cell chaining was accompanied by the convection of the bulk fluid above pH 11 although the rate of convection decreased at higher frequencies.

The effect of pH likely originates from the change in the charge of the cell surface and the concentration and composition of counterions in the double layer. When the pH of the suspension is maintained close to the isoelectric point of pH 4,[54] the decreased number of surface charges leads to a dilute double layer and suppressed polarization. However, at very high (>11) or low (<3) pH values, we see not only chaining but also free convection of the bulk fluid that is due to ac electro-osmotic flows of a large number of negative and positive ions in the system.

Effect of Electrolyte Concentration. Another key parameter that affects the polarization of the counterionic double layer is the electrolyte concentration in the medium. We performed experiments in several different dilutions of PBS. In regular PBS containing ~0.15 M electrolyte, undesirable macroscopic fluid currents were generated because of ac electro-osmosis and water electrolysis. These effects almost completely disappeared below 1.5 mM electrolyte, but this low salt concentration caused osmotic swelling of the mouse fibroblast cells, which eventually began to burst. To compensate for the reduced osmotic pressure outside the fibroblast cell, dextrose was added to the buffer medium. This helped the cells stay viable for a longer time; however, the addition of dextrose slowed the process of cell assembly because of the increase in medium viscosity. There was no need for dextrose addition in the experiments involving yeast cells, which have rigid cell walls and thus remained viable even under the low electrolyte conditions of deionized water. There was a slight but detectable increase in the assembly rate as the electrolyte concentration was decreased further from 1.5 mM to that of deionized water. In summary, the dielectrophoretic assembly of the fibroblast cells can be effectively performed only within a very narrow range of electrolyte concentration, whereas the yeast cells can be assembled in a wide range of electrolyte concentrations similar to the case of synthetic colloidal particles.

Effect of Cell Concentration. The rate of cell assembly increased with the increase in the concentration of cells in the suspension. At higher cell concentrations, the lateral attraction between adjacent cell chains leads to the formation of stripes and partially close-packed 2D arrays extending perpendicular to the direction of the electric field. The transition between such 2D foamlike structures[57] and regular 2D arrays could be achieved only by using the four-electrode cells described later in this article.

Numerical Simulation of Dielectrophoretic Cell Assembly. We developed a model that facilitated the calculation of the magnitudes and direction of the DEP forces involved in the various stages of cell assembly by induced dipolar interactions. Because the magnitude and direction of the DEP force depends on the applied electric field, the electric field distribution in the experimental setup was determined by performing 2D electrostatic calculations in the FEMLAB multiphysics modeling package (COMSOL; Burlington, MA). The spherical cells were modeled in the 2D electrostatic calculations as thin cylinders (or disks) of height h. To represent the system most accurately, the height of the cylinder was chosen to be comparable to the cell diameter ($h=2R$). The electric field distribution was calculated for one positive half cycle of the applied voltage.

The numerical procedure for capturing the experimentally observed cell dynamics using FEMLAB consisted of several steps. The geometry of the system viewed top down was specified to

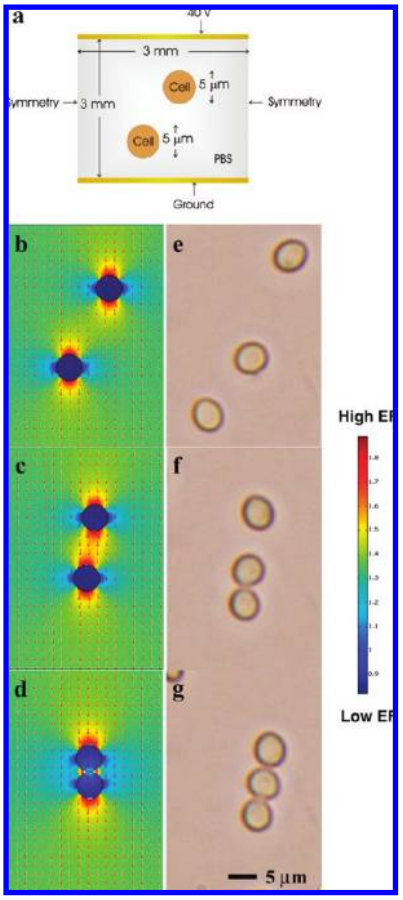

Figure 6. Snapshots of the electrostatic simulation at various stages of cell assembly compared with actual experimental micrographs. The ac electric field is 13 V mm^{-1} and 100 Hz in both cases. (a) Boundary conditions and system geometry specified in the model. (b−d) Time-lapsed simulation of the field and cell rearrangement using FEMLAB. The field intensity is color coded. The higher polarizability of the cells leads to attraction by positive dielectrophoresis. (e−g) Experimental images in transmitted light capturing the dynamics of cell alignment in the ac field.

scale, and the cells were assigned initial coordinates (Figure 6a). The boundaries were the top gold electrode (applied voltage = 40 V) and the bottom gold electrode (ground). The two boundaries to the left and right were taken to be electrically symmetrical. The subdomains consisted of water containing 1.37 mM electrolyte ($\varepsilon_m = 79\varepsilon_0$, $\sigma_m = 0.017$ S) and yeast cells ($\varepsilon_c = 1675.5\varepsilon_0$, $\sigma_c = 0.039$ S). Here, ε_0 is the dielectric permittivity of free space (Table 1). The complex dielectric permittivity and conductivity of yeast cells were calculated using multishell models (modeling details and numerical parameters are given in Supporting Information).[35,58−60] The complex polarizabilities of the media and cells were calculated as a function of frequency, ω, by using the equation $\underline{\varepsilon_{m,c}} = \varepsilon_{m,c} - \frac{j}{\omega}\sigma_{m,c}$.[35]

The computational procedure begins by dividing the solution space into triangular mesh elements. The program was then initialized to solve the Poisson equation ($\nabla^2\phi = -(\rho/\varepsilon_o)$) for all elements in the mesh, and the electric field distribution inside the system was obtained. The electrostatic force vector was generated by the boundary integration of the Maxwell stress tensor on the

(57) Abe, M.; Yamamoto, A.; Orita, M.; Ohkubo, T.; Sakai, H.; Momozawa, N. *Langmuir* **2004**, *20*, 7021–7026.

(58) Sancho, M.; Martinez, G.; Martin, C. *J. Electrostat.* **2003**, *57*, 143–156.

(59) Lyklema, J.; Dukhin, S. S.; Shilov, V. N. *J. Electroanal. Chem.* **1983**, *143*, 1–21.

(60) Lyklema, J.; Springer, M. M.; Shilov, V. N.; Dukhin, S. S. *J. Electroanal. Chem.* **1986**, *198*, 19–26.

Table 2. Force Magnitude Calculations for DEP Interactions between Cells with a Comparison between Numerical and Analytical Values Obtained for Dipolar Forces between Yeast Cells at Two Different Configurations

Dipole Interaction	Center-to-Center Distance between Cells	Numerical Calculations $F_{Num} = -\oint_S \left(-\frac{1}{2}E.D + (n_1.E)D^T\right) dS$	Analytical Calculations $F_{Anal} = C\pi\varepsilon_m Rh\,\mathrm{Re}\left[\left(\frac{\varepsilon_c - \varepsilon_m}{\varepsilon_c + \varepsilon_m}\right)^2\right]E^2$
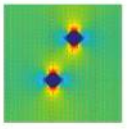	6.7R	3.22×10^{-14} N	3.44×10^{-14} N
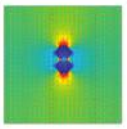	2.0R	1.40×10^{-11} N	6.25×10^{-13} N

exterior surface of each cell ($\vec{F}_{EF} = -(\oint_S(-^1/_2\vec{E}\cdot\vec{D} + (\hat{n}_1\cdot\vec{E})\vec{D}^T)\,dS$). This force was used to calculate the velocity of the cells assuming Stokes-type hydrodynamic resistance, $\vec{v} = \vec{F}_{EF}/6\pi\eta r$. The cells were displaced in a direction and distance determined by the velocity, and their new coordinates were obtained for the next stage of the simulation. The electrostatic field distribution and force vectors were recalculated for the new geometry, and the process was repeated iteratively until the cell boundaries overlapped.

The results of three time-lapsed images at different stages of the simulation performed at 100 Hz are shown in Figure 6b−d. The results illustrate that the electric field intensity is highest above and below the cells in the direction of the electric field, indicating that the cells are more polarizable than the media at this frequency. The high intensities on top and bottom generate local field gradients that attract the cells toward each other by positive DEP and align them collinearly to the field (analogous to dipole−dipole interactions, which in effect are an approximation of the complex calculation performed here). The results of the iteration procedure are in good agreement with the actual experimental observations shown in Figure 6e−g (cf. Supporting Information, movies 1 and 2).

The precision of the numerical procedure was further verified by comparing its results to the analytically calculated magnitude of the dipolar attraction force between two cells using modified eq 3, $F_{chain} = -C\pi\varepsilon_m RhRe|K(\omega)|^2E^2$, where we assume that $h \approx 2R$. The numerical and analytical results for the strength of dipolar attraction between the two cells correlated quite well when the cells were separated by distances greater than ~0.5R (Table 2); a deviation of 1 to 2 orders of magnitude was seen below this gap. This deviation is expected because the analytical dipole−dipole calculations do not account for the higher-order mutual polarization effects that become significant at small interparticle distances and strongly increase the attraction.[35,61] The velocities of the cells after accounting for the hydrodynamic resistance were obtained to be on the order of ~1 μm s^{-1}, which is what we also observe experimentally. These results suggest that the model correctly captures the dynamics and magnitudes of forces involved in the cell-assembly process.

Dielectrophoretic Coassembly of Cell−Particle Binary Systems. The DEP-driven on-chip cell assembly can be of specific value in the co-organization of cells and synthetic particles to form biocomposites, which can be utilized for drug delivery, sensors, components of microsurgery, smart hybrid materials, and others.[4] Because both the chaining and dielectrophoretic forces depend on the size and the material properties of the cells and synthetic particles, a variety of effects can play a role in the coassembly process as well as in the types of structures that are formed. To evaluate the effect of the field on cell−particle mixtures, we examined the dynamics of two kinds of mixed suspensions: (i) cells with similarly sized latex particles and (ii) cells with smaller latex particles.

Binary Suspensions of Cells and Comparably Sized Latex Particles. Latex particles of 5 μm diameter were homogeneously mixed with yeast cells in a 1:1 ratio. This size of latex was chosen in order to eliminate the effect of size and study only the effect of electric polarizability on the coassembly process. Three distinct patterns of chain formation broadly similar to an interaction-induced phase separation were observed when ac fields of strength 4−20 V mm^{-1} and frequency 10−1200 Hz were applied to the mixture (Figure 7). In the indistinguishable mixing region, both the cells and latex spheres were uniformly distributed throughout the length of the chain probably because of similar-strength dipolar interactions. Above 400 Hz and at intermediate field strengths of approximately 12 V mm^{-1}, the proportion of latex spheres in the chains increased dramatically as the cells interacted rather weakly with their neighboring cells and latex particles. This type of cell−particle interaction behavior was termed the transition region. At the highest voltages and frequencies applied above 800 Hz and 16 V mm^{-1}, the cells eventually phase separated from the latex completely and only latex particle 1D chains were left behind.

We believe that the cell/particle segregation above 800 Hz is related to the difference in the relative polarizability of the cells and latex particles as a function of frequency. Under the given experimental conditions, the surface charge densities of the cells and latex are ~0.18 and 3.1 μC cm^{-2}, respectively.[62] These surface charges give rise to a counterionic diffuse double layer that is the major origin of the frequency-dependent, field-induced dipolar polarization.[53,63] At low frequencies, the dipolar polarization induced in both the cells and latex is sufficiently strong to drive the formation of uniformly mixed cell−particle chains. As the

(61) Israelachvili, J. *Intermolecular and Surface Forces*; Academic Press: London, 1992.

(62) The value of the surface charge density of 5 μm latex particles is taken from the information data sheet provided by the vendor, Interfacial Dynamics Corp. (Eugene, OR).

(63) Hoffman, P. D.; Sarangapani, P. S.; Zhu, Y. *Langmuir* **2008**, *24*, 12164–12171.

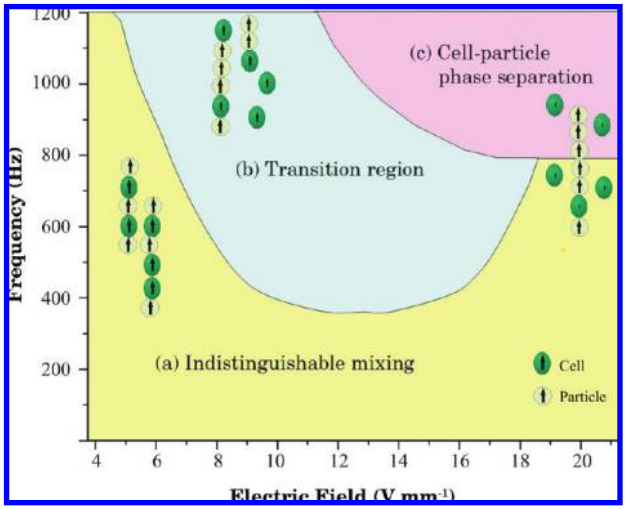

Figure 7. Operational diagram showing the chain morphology of yeast cells and 5 μm sulfate-stabilized latex spheres as a function of field strength and frequency. The different regions in the phase diagram indicate the (a) homogeneous mixing of cells and latex particles through the entire length of the chains; (b) weaker interaction of cells with neighboring cells and latex particles, leading to an increased proportion of latex particles in the chains; and (c) complete phase separation of the cells resulting in latex-particle-only chains.

frequency of the applied field is increased, the polarizability of the cells decreases more rapidly in comparison to that of latex particles. The cells begin to phase separate once the frequency of the field exceeds their characteristic relaxation frequency ($\omega_c \cong$ 800 Hz), but the latex particles continue to form chains. The characteristic relaxation frequency of the latex microspheres was calculated to be $\omega_p \approx 3$ kHz, which lies outside the range of frequencies studied. The lack of phase separation at low voltage for any frequency is probably a result of the weak short-range interactions. When the field strength is very low, the dielectrophoretic and particle chaining forces are too weak to align particles that are farther away than a few particle diameters. Small "chains" of two to three are formed from particles or cells that happen to be in close proximity.

The good correlation between the calculations and experimental data confirms that the coassembly dynamics depends strongly on the complex polarizability of the cells and latex particles. Simulations of the process can predict the types of structures that can be dielectrophoretically assembled from various kinds of cell−particle mixtures.

Binary Suspensions of Cells and Smaller Latex Particles. The coassembly of cells and smaller particles was key to creating biocomposites in which the particles serve as interstitial cell binders. Mixed suspensions comprising 0.2% w/v yeast cells and 0.025% w/v 1.0 μm fluorescent latex particles were prepared and the electric field was applied in the same way as above. ac fields in the low-frequency range of 10−200 Hz always lead to the entrapment of small latex particles between the cell junctions. A typical high-magnification optical micrograph of the cell−particle linear clusters is shown in Figure 8a. A complementary image of this micrograph taken using fluorescence microscopy illustrates how the cells and latex particles are organized into alternating chains (Figure 8b; note that because of the high particle/cell ratio more than one particle is typically captured in each cell−cell junction). Increasing the frequency above 10 kHz resulted in the phase separation of cells and latex (because of the frequency-dependent polarization of the cells and particles described above).

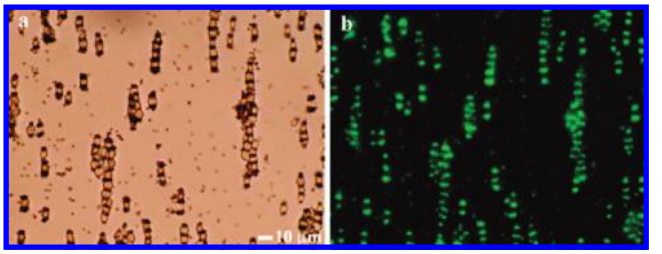

Figure 8. Alternating linear composite clusters of yeast cells (0.2% w/v) and 1 μm green fluorescent latex particles (0.025% w/v) assembled at 15 V mm^{-1} in a 200 Hz ac electric field. (a) Optical micrograph taken after the field was applied for 45 min. (b) Complementary image of the system in panel a acquired using fluorescence microscopy. The green fluorescent stripes reveal the positions of the latex microparticles captured in between the cells.

The phenomenon of latex particle entrapment between cells was mostly observed at low electrolyte concentrations; increasing the electrolyte concentration suppresses the coassembly process.

To understand better the role of the electric field in cell−particle chain formation, the coassembly dynamics was simulated in FEMLAB using the model developed above for the field-induced interaction between two cells (as in Figure 6). To simplify the complex calculations, the experiment was represented by a 2D system consisting of only two cells and two latex particles placed between parallel coplanar electrodes (Figure 9a). The dielectric permittivity and conductivity of 1.0 μm latex particles ($\varepsilon_p = 2.55\varepsilon_0$, $\sigma_p = 0.02$ S) were calculated by using multishell models (detailed calculations and numerical parameters in Supporting Information).[56,64,65] The complex permittivity values for yeast cells and PBS media were the same as in the simulations of cell−cell interactions. The calculations were performed for a constant applied field corresponding to one positive half cycle.

Sequential time-evolved images of the electric field distribution and particle rearrangement at various stages of the assembly are presented in Figure 9b−e. The field strength and frequency were 13.3 V mm^{-1} and 100 Hz, respectively. Both the 1.0 μm particles and the cells are more polarizable than the medium under the given conditions. The electric field draws the small particles by positive dielectrophoresis toward the regions of highest localized field intensities that exist directly above or below the cells (along the direction of the field). This in turn attracts the next cell, and as a result, the latex particle gets trapped between the cells. The capture of smaller latex particles between cells is thus a field-driven process. This simulation corresponds very well to the experimentally observed coassembly dynamics in similar cell−particle configurations (cf. Supporting Information movies 3 and 4). We have also observed other routes of assembly depending on the initial positions of the cells and latex particles (i.e., the cells can also first be drawn toward each other and then the particles are captured between them (results not shown here)); however, the final structure always consists of particles trapped in between the cells in the chains. This allows us to turn these assemblies into permanent structures.

Permanent Cell Chains Using Functionalized Microparticles and Ligands. The electric field plays a key role in forming various architectures of cell−cell and cell−particle chains, the morphology of which can be controlled by a few simple parameters. However, these assemblies are not permanent and therefore cannot be employed in useful functional materials. Because

(64) Green, N. G.; Morgan, H. *J. Phys. Chem. B* **1999**, *103*, 41–50.
(65) Arnold, W. M.; Schwan, H. P.; Zimmermann, U. *J. Phys. Chem.* **1987**, *91*, 5093–5098.

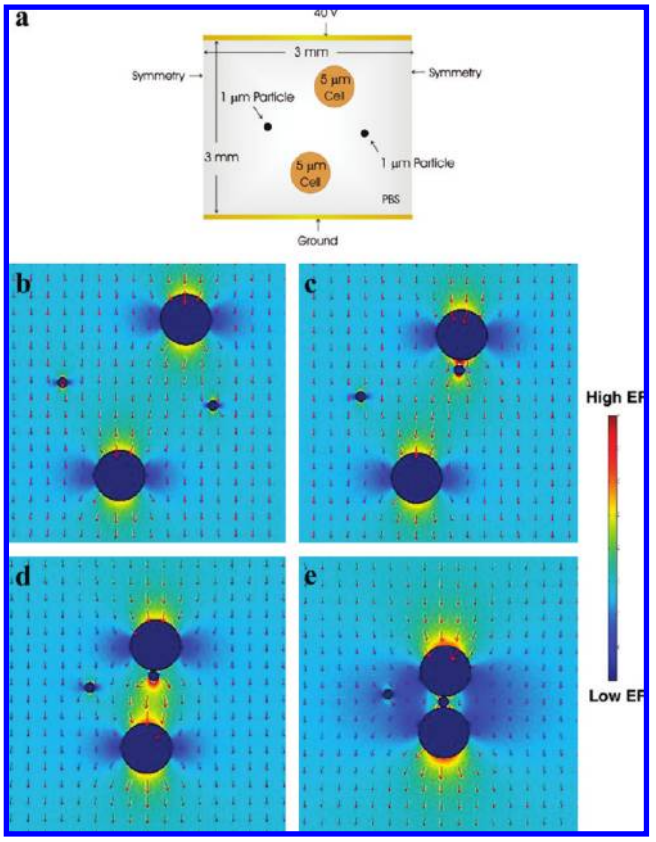

Figure 9. Snapshots of the electrostatic simulation of the various stages of cell−particle coassembly calculated in a field of 100 Hz. (a) Specifications of the system geometry and boundary conditions used in the model. (b−e) Time-lapse simulation of the field intensity distributions and cell−particle rearrangement using FEMLAB. The areas of highest local field intensity above and below the cells (collinear with the field) attract the particles by positive dielectrophoresis, leading to the formation of alternating cell−particle linear chains.

the latex particles can be dielectrophoretically incorporated between the cells during our field-driven coassembly process, we can design the small particles to serve as "biocolloidal glue" if their surfaces are functionalized with a ligand that binds irreversibly to the cell surfaces. This could allow not only the assembly of permanent biocomposites but also the engineering of the specific functionality of the hybrid biomaterial by synergistically combining the property of the binder particles to those of the cells.[46]

We performed experiments in which different types of ligand-functionalized organic and inorganic microparticles were used as permanent binding units. The binding of the cells and the particles was accomplished mainly by two types of interactions: electrostatic and biospecific (Figure 10a,b). For the electrostatic binding

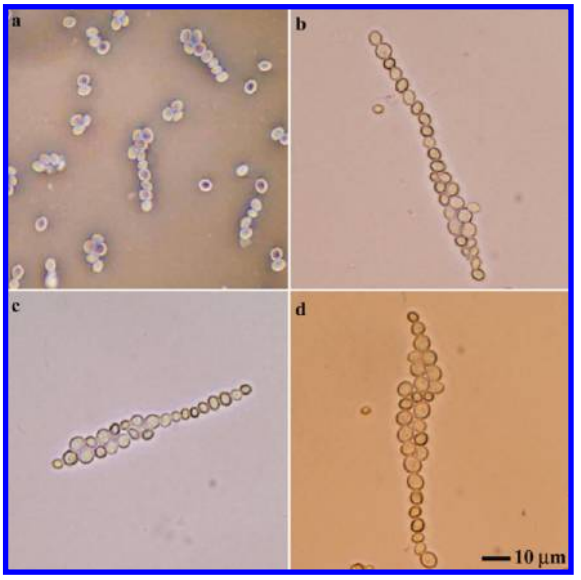

Figure 11. Permanent binding of yeast cell chains after DEP assembly using (a) poly(dimethyl aminoethyl methacrylate) (PDMAEMA), (b) concanavalin-A, (c) D-mannose, and (d) both concanavalin-A lectin and D-mannose.

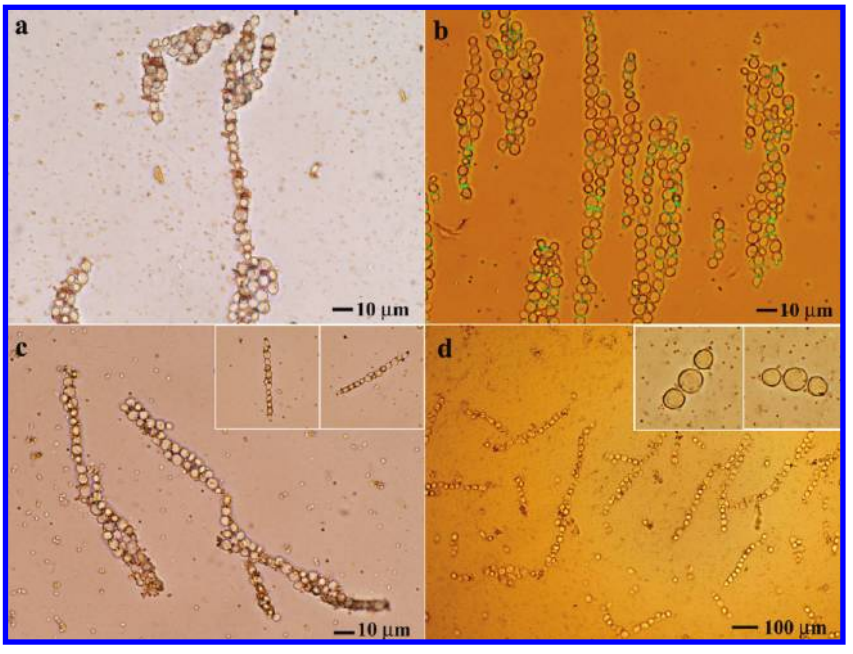

Figure 10. DEP assembly of permanent cell chains using functionalized binder particles. (a) Yeast cells with 1.8 μm amine-terminated iron oxide particles. (b) Yeast cells with 1.0 μm lectin-coated fluorescent latex particles. (c) Yeast cells with 0.95 μm lectin-coated magnetic particles. (d) Mouse fibroblast cells with 0.95 μm lectin-coated magnetic particles. The insets show chain rotation using an external magnet.

Table 3. Summary of the Results for Binding Experiments Performed with Yeast and Fibroblast Cells[a]

types of binders	concentration of binding agents	approx. time of EF (min)	result for permanent binding: with yeast	result for permanent binding: with fibroblast
		Functionalized Particles		
1.8 μm amine-terminated particles	0.013 − 0.036% w/v	10	√	√
1.0 μm fluorescent aldehyde/sulfate latex	0.02% w/v	45	√	
1.0 μm lectin-coated fluorescent latex	0.025% w/v	45	√	
1.0 μm lectin-coated fluorescent latex + D-mannose	0.025% w/v + 60 mM	45	√	
1.8 and 0.95 μm lectin-coated particles	0.017 − 0.018% w/v	60	√	√
		30		
1.8 μm and 0.95 lectin-coated particles + D-mannose	0.013% w/v + 38 mM	30	√	
1.0 μm fibronectin-coated latex	0.016% w/v	45		√
		Ligands		
PDMAEMA	7.5×10^{-4} % w/v	30	√	
lectin	5×10^{-4} % w/v	60	√	
D-mannose	43.5 mM	30	√	
lectin + D-mannose	5×10^{-4} % w/v + 60 mM	45	√	
		Controls		
1.0 μm sulfate-stabilized polystyrene latex	0.013% w/v	60	×	
1.8 μm amine-terminated particles + excess BSA	0.013% w/v	60	×	

[a] The concentration of cells is between 0.01 and 0.2% w/v. The applied field parameters were 5−17 V mm^{-1} and 50−10 kHz. Symbols √ and × represent permanent binding and no permanent binding, respectively. A blank means no experiment was performed.

of negatively charged cells, we used positively charged 1.8 μm iron oxide particles with amine end groups. When an ac field was applied to the cell−particle mixtures, the binder particles were invariably captured between the cells and irreversibly attached to them in less than 10 min. Though this process yielded permanent chains, it was difficult to prevent their adhesion to the negatively charged glass surface. The problem of surface adhesion was overcome by using 1.0 μm FITC-labeled fluorescent microparticles, which had chemically attached lectins on their surfaces. Lectin is a type of protein that binds biospecifically to the saccharide functional groups on the cell surface in the presence of a small number of Ca^{2+} ions.[47] Permanent binding of cells by concanavalin A lectin was achieved in 30−45 min. The morphology of the cell chains could also be controllably modified in every experiment. For example, chains prepared with a higher ratio of particles to cells were more rigid. Also, chains formed at smaller frequencies were longer (consistent with our previous results).

We further demonstrated that one can make responsive cell−particle "wires" by using binder particles that have an intrinsic magnetic functionality. For instance, permanent chains containing either yeast or mouse fibroblast cells were assembled with the mediation of 0.95 μm lectin-coated paramagnetic particles. These chains could then be transported and rotated in seconds by magnetophoretic torque in the field of a small permanent magnet (Figure 10c,d). The chains remained intact even in the presence of shear flow during the manipulation and were stable over a period of a few days following the experiment.

The permanent binding of cells alone could alternatively be performed by using molecular binding ligands. We demonstrated this by using three different kinds of ligands that attached to the cells through either electrostatic or biospecific interactions (Figure 11). Positively charged polymer poly(dimethyl aminoethyl methacrylate) (PDMAEMA) electrostatically attached to the negatively charged yeast cells, but it was again difficult to prevent the chains from adhering to the glass substrate. Lectin (Concanavalin A) and D-mannose, however, initiated irreversible biospecific attachment by binding to polysaccharides present on the cell wall or triggering constituent carbohydrate receptors, respectively.[66,67] The results from these and from a few other additional binding and control experiments are summarized in Table 3.

Assembly of 2D Cell Arrays. In addition to assembling 1D chains and wires, we also demonstrated the ability to assemble the cells into 2D arrays. Our previous results for the 2D crystal assembly of latex and silica particles using a two-electrode chip have shown that the crystallization process proceeds in two stages.[43,44] In the first stage, particle chains are formed because of attractive induced-dipole interparticle interactions. In the second stage, the lateral interaction between the dipoles in the adjacent particle chains assembles hexagonally close-packed 2D crystals. When we used the two-electrode chip in our initial attempt to form cell 2D arrays, we observed that the cells formed 1D chains (similar to those observed with latex and silica particles) but the lateral dipolar and multipolar interactions between the cell chains were too weak to assemble the chains into long-range 2D arrays (Figure 12a). We believe the reasons for the lack of attraction between cell chains are that the cells are polydisperse and they polarize weakly in comparison to the microparticles.

To overcome the problem of packing weakly interacting inhomogeneous particles, we designed a four-electrode experimental setup. The chip with four orthogonally arranged point electrodes allowed us to apply the electric field in two perpendicular directions (Figure 2b). The voltage source could be connected to any pair of adjacent electrodes. The ac field was first applied to the cell suspension in one direction for ~15 min. By the end of this period, the cells settled at the bottom of the chip and aligned in the direction of the electric field via axial dipolar interactions. The field was then switched to the other electrode pair to let the cells realign along the perpendicular direction. The switching process was repeated approximately every 5 min for a total duration of 30−45 min until we managed to draw the cells into uniformly close-packed arrays (movie 5 in Supporting Information).

(66) Sharon, N.; Lis, H. *Science* **1972**, *177*, 949–959.
(67) Lis, H.; Sharon, N. *Chem. Rev.* **1998**, *98*, 637–674.

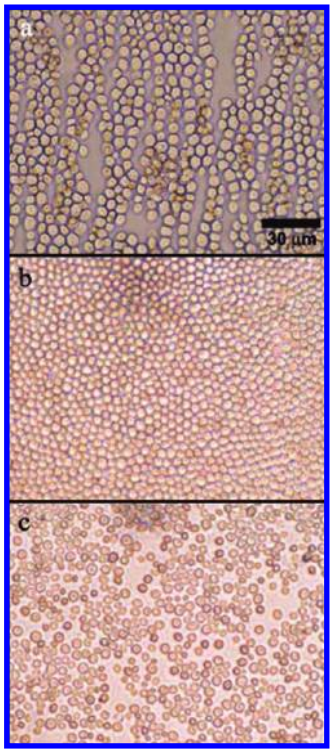

Figure 12. Two-directional alignment and annealing in ac fields for the assembly of uniform 2D cell arrays. (a) No close-packed 2D yeast cell array was obtained using two parallel coplanar electrodes. (b) Organization of yeast cells into close-packed 2D arrays using the four-point electrode setup. The field was applied for 30 min. (c) Random deposition of yeast cells that had freely sedimented under a gravity-only force (no electric field) for 30 min.

A high-magnification optical micrograph of a single-layer 2D array of yeast cells assembled in 30 min using the four-electrode chip is shown in Figure 12b. The volume fraction of the cell suspension was 0.08% w/v (adequate to form a monolayer). To confirm that the on-chip field-driven process is essential to the formation of close-packed 2D arrays, we performed in parallel a control test in which the same concentration of yeast cells was allowed to sediment freely under gravity (without an electric field) for 30 min in the same experimental cell (Figure 12c and movie 6 in Supporting Information). No close-packed 2D cell structure was obtained in the absence of the electric field, which proved that the two-directional alignment and annealing in ac fields was the main driving force for the formation of close-packed 2D arrays of cells.

DEP Assembly of Magneto-Responsive Permanent Cell Membranes. The cell−particle chaining experiments proved that the capture of functionalized binder particles between cells during the process of field-induced organization is critical to the irreversible biocomposite assembly. That approach combined with the 2D assembly technique was extended to the fabrication of permanent, responsive biomembranes. Mixed suspensions of cells and lectin-coated magnetic particles were coassembled into large ($\sim$cm^2) permanent magnetic membranes using the four-electrode chip (Figure 13). A field-emission scanning electron microscopy (FESEM) image of a yeast cell membrane fixed with glutaraldehyde showed that the particles were embedded between the closely packed cells (Figure 13a).

The biomembranes assembled on the chip were rotated, folded, and translated in 2D and 3D using external magnetic fields (Figure 13b,c) (movies 7 and 8 in Supporting Information). We

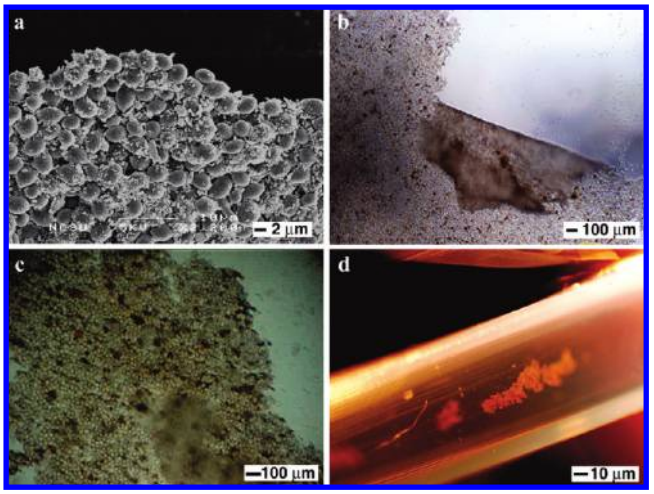

Figure 13. Magnetically responsive cell membranes assembled in a four-electrode DEP cell. (a) FESEM scanning electron micrograph of a closely packed permanent yeast cell membrane bound together by 0.95 μm concanavalin-A-functionalized magnetic particles. The membrane was fixed with 2% w/v glutaraldehye and sputtered with gold for the preparation of the SEM sample. (b) Folding of a yeast cell membrane using an external magnet. The cells are irreversibly bound by 0.95 μm lectin-functionalized particles. (c) Snapshot of a freely suspended fibroblast cell membrane being dragged and transported in an external magnetic field. (d) Magnetic transportation of a yeast cell membrane through Teflon tubing connected to the DEP flow chamber.

were also able to demonstrate that the membranes could be removed from the chips where they were assembled and transported to the site of further use. For this purpose, thin, transparent Teflon tubing was interfaced to the four-electrode microchamber and the membranes flowed out of it using the pull of a small magnet (Figure 13d). The ability to manipulate these live cellular membranes using external magnetic fields could be harnessed for biomedical applications that require the rapid orientation and replacement of cell patches that may serve as artificial tissues for microsurgery and prosthetics. It is likely that the cells will retain their viability in the structures over long times; however, the lifetime of the cells in these heterostructures is an important issue that has yet to be characterized.

4. Conclusions

We demonstrate that ac electric fields are a precise tool for the rapid and directed coassembly of live cells and synthetic colloidal particles into freely suspended biocomposites. Operating conditions such as the electrode geometry, voltage and frequency of the applied field, pH, electrolyte and cell concentration in the buffer media, and particle size are shown to be essential in controlling the rate of assembly and the morphology of the resulting structures. Experimental observations and electrostatic simulations of the cell−particle coassembly dynamics illustrate that at low frequencies smaller synthetic particles are captured in between the cell junctions by positive dielectrophoresis. By using this effect to capture various types of surface-functionalized colloidal particles, we have demonstrated how permanent cell structures can be assembled on a chip. The utilization of lectin-coated paramagnetic particle binders allowed the fabrication of stable, responsive cell wires and cell membranes that could be freely manipulated inside the chip and extracted by using external magnetic fields. One potential application of these magnetic composite materials could be in real-time biosensors fabricated by using external magnetic fields for the rapid alignment of the cell wires between

 DOI: 10.1021/la902989r K

micropatterned electrodes. These novel functional biocomposites also hold promise for prosthetics and drug delivery systems.[68−72] The on-chip DEP technique could easily be extended to other systems in which the electrical, optical, or any other functionality of the binder particles could be combined with the cell function to create smart materials.[4,37]

(68) Pappas, T. C.; Wickramanyake, W. M. S.; Jan, E.; Motamedi, M.; Brodwick, M.; Kotov, N. A. *Nano Lett*. **2007**, *7*, 513–519.
(69) Shipway, A. N.; Katz, E.; Willner, I. *Chem. Phys. Chem*. **2000**, *1*, 18–52.
(70) Beck, J. D.; Shang, L.; Marcus, M. S.; Hamers, R. J. *Nano Lett*. **2005**, *5*, 777–781.
(71) Collier, J. H.; Mrksich, M. *Proc. Natl. Acad. Sci. U.S.A*. **2006**, *103*, 2021–2025.
(72) Jung, D. R.; Cuttino, D. S.; Pancrazio, J. J.; Manos, P.; Cluster, T.; Sathanoori, R. S.; Aloi, L. E.; Coulombe, M. G.; Czarnaski, M. A.; Borkholder, D. A.; Kovacs, G. T. A.; Bey, P.; Stenger, D. A.; Hickman, J. J. *J. Vac. Sci. Technol., A* **1998**, *16*, 1183–1188.

Acknowledgment. We thank Michael Weiger and Jason Haugh at NCSU for generously providing the NIH/3T3 mouse fibroblast cells, Jan Genzer's laboratory for providing PDMAEMA, Anka Veleva for access to ImagePro software, Erik Santiso for scientific discussions, and Valerie Knowlton and Dale Batchelor for assistance with the SEM imaging. This study was supported by NIRT grants (0506701 and 0609087) from the National Science Foundation.

Supporting Information Available: Movies illustrating the field-assisted assembly and manipulation of cells and particles into chains and membranes, protocols for protein conjugation to colloidal particles, and analytical calculations of yeast cell and latex particle polarizabilities using multishell models. This material is available free of charge via the Internet at http://pubs.acs.org.